Decentralized Cooperative Control of Unmanned Aerial Vehicles Based on Emergent Mechanism of Starlings

*MEI Yu, DUAN Haibin**

National Key Laboratory of Aircraft Integrated Flight Control, School of Automation Science and Electrical Engineering, Beihang University, Beijing 100083, P. R. China

(Received 10 December 2025; revised 25 February 2026; accepted 1 March 2026)

Abstract: A novel decentralized control approach for unmanned aerial vehicles (UAVs) based on emergent collective behavior identified in starling flocks is proposed in this paper. With the self-organizing principle of starling flocking separation, alignment and cohesion behaviors, a fully distributed leaderless control is designed based on local interaction only. It is augmented by an adaptive switching event-triggered communication protocol, a novelty which greatly reduces the communication load, yet maintains swarming cohesion and formation stability rigorously. Via the Lyapunov stability theory, the formation error can converge to a boundary range, robustness to disturbances and partial communication burden. Ultimately, the numerical simulations are presented to verify the effectiveness of the theoretical results.

Key words: starling flocking; decentralized control; switching event-triggered communication; ummanned aerial vehicle (UAV) swarm control

CLC number: TP271 **Document code:** A **Article ID:** 1005-1120(2026)02-0145-13

0 Introduction

In recent decades, drawing inspiration from the flocking of starlings, the investigation of unmanned aerial vehicles (UAVs) collaboratively is a rapidly growing field of study. The technical superiority of UAVs formations in wide areas, such as surveillance[1], collaborative mapping[2], communication network[3], is well established, deriving primarily from their unsurpassed parallel tasking capability, high inherent redundancy-based robustness and flexible scalability. Thus, a central challenge lies in enabling a collection of resource-limited autonomous agents to exhibit intelligent global coordination using only local sensing and communication.

Starling flocks exhibit highly coordinated, adaptive, and resilient dense flocking maneuvers, a phenomenon termed murmurations, which have no leader. Among them, each individual flies solely by following dynamic information from its neighbors. Based on these simple local rules, the group achieves complex collective motions and rapid changes in morphology[4], which offers a strong biological inspiration to design distributed and scalable control algorithms for UAVs. The local rules, such as separation, collision avoidance, alignment of direction, displayed by bird flocks were developed into the boids model by Reynolds et al.[5], which was the first to reproduce the emergence of collective intelligence through computational means. This model was later systematically applied and evolved into a unity framework for multi-agent distributed control. The method based on the consistency theory gradually matured and became one of the main approaches for dealing with formation control problems[6]. Further inspired by this, consensus-based control methods, based on boids models or its theoretical extensions, are canonical and popular tools

*Corresponding author, E-mail address: hbduan@buaa.edu.cn.

How to cite this article: MEI Yu, DUAN Haibin. Decentralized cooperative control of unmanned aerial vehicles based on emergent mechanism of starlings[J]. Transactions of Nanjing University of Aeronautics and Astronautics, 2026, 43(2): 145-157.

http://dx.doi.org/10.16356/j.1005-1120.2026.02.001

for the multi-agent formation problem[7-8]. This is one of the motivations of this paper.

Considerable research attentions have been focused on the development of formation control strategies for UAVs. Ma et al.[9] proposed an integrated localization and motion planning scheme for multi-UAV networks to analyze error bounds and enhance formation accuracy under measurement and motion noises. Khodaverdian et al.[10] designed dual-loop control architecture to address the trajectory-following problem for multiple fixed-wing UAVs with high nonlinearity and strong coupling, which separates the dynamics into two subsystems and integrates nonlinear model predictive control with fault-tolerant sliding mode predictive control. Zhou et al.[11] proposed an enhanced marine predators algorithm with a receding horizon control framework to address the constrained, high-dimensional nonlinear optimization problem in UAV formation reconfiguration, offering stronger optimization capability, greater stability, and improved real-time performance. However, given the tight communication and energy budgets of quadrotor UAVs, the time-triggered control strategies discussed above prove to be suboptimal for endurance-critical tasks. There has been a common drawback on such strategies which relies on continuous or periodic communication, leading to network congestion and resources wasting[12].

Traditional time-sampling approaches are prone to generating significant data redundancy, which can cause network congestion and potential collapse. Consequently, the event-triggered control (ETC) strategy has attracted considerable research interests, with its mechanism of transmitting measurement signals only upon meeting predefined trigger conditions. Dimarogonas et al.[12] proposed a distributed event-triggered control framework, achieving coordinated consistency. Different from the traditional time-triggered mechanism, this approach effectively alleviates network load. Based on the triggering mechanism, ETC strategies are broadly categorized into the following types, fixed-threshold ETC, relative-threshold ETC[13-15], dynamic ETC[16-18], and self-triggering ETC[19-20]. Subsequent research also furthered the development of ETC. To further reduce data transmission, an internal dynamic variable was introduced based on the traditional ETC, thereby constructing a dynamic event triggering mechanism (DETM)[21-22]. To address specific robustness challenges, the hybrid switching ETC has also been proposed. For instance, to ensure strict positive minimum event intervals in the presence of interference[23] or to guarantee the safety and stability of the formation when facing network threats such as replay attacks[24], denial-of-service attacks[25].

For example, Shi et al.[26] designed an improved integral ETC mechanism for time-varying formation tracking, which significantly reduced the triggering frequency compared to conventional methods while ensuring bounded tracking error via a multi-Lyapunov function approach. Huang et al.[27] investigated the formation control problem for quadrotor UAVs under switching directed topologies, proposing a distributed event-triggered algorithm via a hierarchical framework that solely relies on neighbors' position information and maintains smooth performance amidst discontinuities. Liu et al.[28] developed a switching-based fault-tolerant control scheme for multi-agent systems with disturbances and actuator faults, which ensured that reverse faults were handled without invalid switching or excessive control shocks, while a conditional compensation mechanism guaranteed smaller steady-state error and reduced energy consumption by utilizing beneficial disturbances. The above-mentioned ETC mechanism has indeed significantly reduced the communication burden. However, a single change is not sufficient to handle unexpected situations during UAVs' flight. Therefore, establishing a switching ETC mechanism is also one of the motivations of this paper.

Inspired by these observations, a novel decentralized control approach for UAVs based on emergent collective behavior seen in starling flocks with switching ETC mechanism is proposed. In comparison to the aforementioned studies, the principal innovations of this paper are outlined as follows.

(1) A unified decentralized control paradigm that combines the self-organizing principles of starling flocks and switching ETC mechanism is proposed to addresses the critical trade-off between formation stability and communication efficiency in UAV swarms.

(2) The design and theoretical verification of the novel switching event-triggered mechanism. Unlike conventional periodic or fixed-threshold triggering, this protocol dynamically adjusts communication based on real-time cohesion needs.

Table 1 provides a comprehensive comparison and summary of the proposed method and similar previous works. The rest of this paper is arranged as follows. Section 1 shows the system model and problem description. The control law inspired by starling flocking rules and switching event-triggered mechanism are introduced in Section 2. The stability analysis of the closed-loop system dynamics is presented in Section 3. Section 4 presents two simulation examples as we have demonstrated, and the conclusions are drawn in Section 5.

Table 1 Comparative summary of the proposed method and previous works

Reference	Control method	Communication strategy	Robustness	Main limitations
[5]	Classic boids model	Continuous	—	High costs
[6]	Flocking consensus	Continuous/periodic	Network connectivity	Fixed frequency
[12	Multi-agent consistency	Fixed threshold	Bounded perturbation	Poor adaptability
[21]	Distributed observer	Relative threshold	Time-varying delay	Fixed topology
[22	Reinforcement learning	State dependent triggering	Unknown nonlinearity	Model limitation
[23	Predictive control	Continuous/periodic	Bounded perturbation	Non-fully distributed
[24]	Distributed observer	Switching threshold	Packet loss	Attack alone
[25]	Distributed observer	Relative threshold	Targeted DOS attack	Offline distributed
Proposed method	Improved boids model	Mode switching threshold	Disturbance fault	Moderate complexity

1 System Model and Problem Description

1.1 UAV dynamic model

Consider a swarm system consisting of N UAVs. Each UAV is modeled as a double integrator, widely used in formation control research due to its effectiveness in capturing the double-integrator relationship between position and velocity, while facilitating theoretical analysis[5]. The dynamics of the ith UAVs are described as

$$\begin{cases} \dot{\boldsymbol{p}}_i = \boldsymbol{v}_i \\ \dot{\boldsymbol{v}}_i = \boldsymbol{u}_i + \boldsymbol{d}_i(t) \end{cases} \tag{1}$$

where $\boldsymbol{p}_i \in \mathbf{R}^3$ and $\boldsymbol{v}_i \in \mathbf{R}^3$ denote the position and velocity vectors of UAVi in 3D space, respectively; $\boldsymbol{u}_i \in \mathbf{R}^3$ is the control input to be designed; $\boldsymbol{d}_i \in \mathbf{R}^3$ the aggregate effect of realistic uncertainties, including communication imperfections and modeling errors. We characterize these disturbances by condition $\|\boldsymbol{d}_i(t)\| \leqslant d_{\max}$, where $d_{\max} > 0$ serves as a known constant upper bound ensuring the system's resilience. This model assumes that the inner-loop attitude controller of the UAV can perfectly track velocity commands, allowing the focus to remain on the design of the outer-loop formation controller.

1.2 Communication topology model

Information interaction among UAVs is described by a time-varying undirected graph $\mathcal{G}(t) = (\mathcal{V}, \mathcal{E}(t))$, where $\mathcal{V} = \{1, 2, \cdots, N\}$ is the node set, and $\mathcal{E}(t) \subseteq \mathcal{V} \times \mathcal{V}$ is the time-varying edge set. An edge $(i, j) \in \mathcal{E}(t)$ exists if UAVj is within the communication range of UAVi. The neighbor set of UAVi is defined as $\mathcal{N}_i(t) = \{ j \in \mathcal{V} : (i, j) \in \mathcal{E}(t) \}$. We assume the initial graph $\mathcal{G}(0)$ is connected. The Laplacian matrix $\boldsymbol{L}(t) = [l_{ij}(t)] \in \mathbf{R}^{N \times N}$ associated with $\mathcal{G}(t)$ is defined as: If $i = j$, $l_{ij}(t) = |\mathcal{N}_i(t)|$; if $j \in \mathcal{N}_i(t)$, $l_{ij}(t) = -1$; otherwise $l_{ij}(t) = 0$. The algebraic connectivity $\lambda_2(\boldsymbol{L}(t))$ of the Laplacian matrix is crucial for analyzing the convergence proper-

ties of system (1).

Lemma 1[29] For any given positive constants r_1, r_2 and r_3, it holds that

$$|x|^{r_1}|y|^{r_2} \leqslant \frac{r_1}{r_1+r_2} r_3 |x|^{r_1+r_2} + \frac{r_2}{r_1+r_2} r_3^{-\frac{r_1}{r_2}} |y|^{r_1+r_2}$$

where x and y are any real variables.

1.3 Control objectives and problem statement

This paper aims to design a fully distributed control law $\boldsymbol{u}_i(t)$ for each UAVi, which can only access the state information of its neighbors $j \in \mathcal{N}_i(t)$, to achieve the following three core objectives.

(1) Formation acquisition and maintenance: Guide all UAVs to converge to and maintain a predefined geometric configuration. That is, there exists a set of fixed desired relative displacements $\boldsymbol{d}_{ij} \in \mathbf{R}^3$, satisfying $\boldsymbol{d}_{ij} = -\boldsymbol{d}_{ij}$ and $\boldsymbol{d}_{ii} = 0$, such that the position vectors of all UAVs converge to $\lim_{t\to\infty}(\boldsymbol{p}_i(t) - \boldsymbol{p}_j(t) - \boldsymbol{d}_{ij}) = 0$.

(2) Velocity consensus: This requires the asymptotic convergence of all UAV velocities to a common vector, ensuring the condition $\lim_{t\to\infty}(\boldsymbol{v}_i(t) - \boldsymbol{v}_j(t)) = 0$.

(3) Resilience and communication efficiency: Maintain system stability in the presence of external disturbance. Simultaneously, the control algorithm should significantly reduce unnecessary communication to conserve valuable onboard communication resources.

2 Controller Design

2.1 Control law inspired by starling flocking rules

Drawing inspiration from the flocking behavior of starlings, we formulate a control law that integrates the essential rules of separation, alignment, and cohesion, following the schematic shown in Fig.1.

Unlike the classical boids model, a tracking term is introduced for the desired formation $\boldsymbol{d}_{ij}$ and computeed using estimated states of neighbors. For UAVi, its control input $\boldsymbol{u}_i$ is designed as

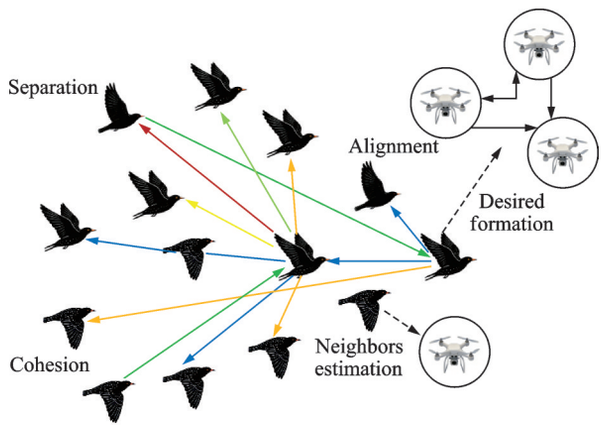

Fig.1 Schematic diagram of starling-inspired UAV formation control architecture

$$\boldsymbol{u}_i = -k_s \sum_{j\in\mathcal{N}_i(t)} \phi_s(\|\boldsymbol{p}_{ij}\|) \nabla_{\boldsymbol{p}_i} - k_a \sum_{j\in\mathcal{N}_i(t)} a_{ij}(\boldsymbol{v}_i - \hat{\boldsymbol{v}}_j) - k_c \sum_{j\in\mathcal{N}_i(t)} \left((\boldsymbol{p}_i - \hat{\boldsymbol{p}}_j) - \boldsymbol{d}_{ij}\right) \tag{2}$$

where $\boldsymbol{p}_{ij} = \boldsymbol{p}_i - \boldsymbol{p}_j$; $\phi_s(r) = 1/r^2 - 1/r_0^2$ is a smooth repulsive potential function, with $r_0 > 0$ being a preset safety distance, and it ensures a safe inter-agent distance to prevent collisions; $k_s, k_a, k_c > 0$ are tunable control gains weighting the influence of the three rules; $\hat{\boldsymbol{p}}_j$ and $\hat{\boldsymbol{v}}_j$ the estimated states of neighbor j held by UAVi, updated via the event-triggered communication mechanism; and a_{ij} is the adjacency matrix element.

2.2 Switching event-triggered mechanism

To reduce communication burden, UAVs do not broadcast their states periodically. Instead, communication occurs only when a locally measured state estimation error exceeds a certain threshold. This threshold can switch between a fixed value and a dynamic one based on system performance, enhancing adaptability. The state estimation error for UAVi at time t is defined as

$$\begin{cases} \boldsymbol{e}_{p_i} = \boldsymbol{p}_i(t) - \hat{\boldsymbol{p}}_i(t) \\ \boldsymbol{e}_{v_i} = \boldsymbol{v}_i(t) - \hat{\boldsymbol{v}}_i(t) \end{cases} \tag{3}$$

where $(\hat{\boldsymbol{p}}_i(t), \hat{\boldsymbol{v}}_i(t))$ are the most recently broadcast values of UAVi own state to its neighbors. For a neighbor j of UAVi, UAVi uses its stored values $(\hat{\boldsymbol{p}}_i(t), \hat{\boldsymbol{v}}_i(t))$ to compute the control law. The event-triggering condition is designed with a switching mechanism

$$\| \boldsymbol{e}_{p_i}(t) \|^2 + \gamma \| \boldsymbol{e}_{v_i}(t) \|^2 \geqslant \delta_i(t) \tag{4}$$

where $\gamma > 0$ is a weighting coefficient. $\delta_i(t) > 0$ is a switching threshold

$$\delta_i(t) = \begin{cases} \alpha e^{-\beta t} + \delta_{\min} & E_i(t) > \eta \\ \delta_{\mathrm{f}} & E_i(t) \leqslant \eta \end{cases} \tag{5}$$

where $E_i(t) = \| \boldsymbol{e}_{p_i}(t) \| + \| \boldsymbol{e}_{v_i}(t) \|$ is a local performance metric; and $\eta > 0$ a switching parameter. In dynamic mode, $\alpha, \beta > 0$ control the decay rate, and $\delta_{\min} > 0$ is a positive lower bound that ensures that events are not triggered infinitely fast. In the fixed mode, $\delta_{\mathrm{f}} > 0$ is a constant threshold. This design allows the aggressive error reduction to be initial and stable, and low-frequency triggering near equilibrium.

When the inequality holds, UAVi triggers an event: It immediately broadcasts its true state $(\boldsymbol{p}_i(t), \boldsymbol{v}_i(t))$ to all neighbors and updates its own estimated value $(\hat{\boldsymbol{p}}_i(t), \hat{\boldsymbol{v}}_i(t))$. Upon receiving this information, neighbor j updates its stored estimate for i. At non-triggering instants, all UAVs use the last received neighbor state estimates for computation. This mechanism effectively reduces communication frequency, especially when the system is near steady state.

Remark 1 The parameters in Eq.(5) have clear physical meanings and can be systematically selected based on experience. The fixed threshold δ_{f} primarily governs the communication rate during transient phases. It should be selected based on the allowable communication bandwidth. Specifically, a larger δ_{f} reduces the data exchange frequency but may slow down convergence. The coefficients α and β regulate the adaptation speed of the threshold. α scales the influence of the performance metric, while β controls the exponential decay rate. To ensure the threshold does not collapse too quickly to $\delta_{\min}$, $\beta \in (0, 1)$ is recommended to be set. The parameter η adjusts the sensitivity of the trigger to the estimation error. A larger η makes the system more sensitive to errors, suitable for highly dynamic scenarios, whereas a smaller η favors energy saving.

3 Stability Analysis

3.1 Closed-loop system dynamics

For analysis convenience, we define the formation tracking error and velocity consensus error

$$\boldsymbol{q}_i = \boldsymbol{p}_i - \boldsymbol{p}_i^{\mathrm{d}} \qquad \boldsymbol{w}_i = \boldsymbol{v}_i - \boldsymbol{v}_i^{\mathrm{d}} \tag{6}$$

where $\boldsymbol{p}_i^{\mathrm{d}}$ is the desired position of UAVi, satisfying $\boldsymbol{p}_i^{\mathrm{d}} - \boldsymbol{p}_j^{\mathrm{d}} = \boldsymbol{d}_{ij}$; and $\boldsymbol{v}^{\mathrm{d}}$ the desired common velocity. Through introducing the error variable, the control law (2) can be expressed as

$$\begin{aligned} \boldsymbol{u}_i = & -k_{\mathrm{s}} \sum_{j \in \mathcal{N}_i(t)} \phi_{\mathrm{s}}(\| \boldsymbol{p}_{ij} \|) \nabla_{\boldsymbol{p}_i} - k_{\mathrm{a}} \sum_{j \in \mathcal{N}_i(t)} (\boldsymbol{w}_i - \hat{\boldsymbol{w}}_j) - \\ & k_{\mathrm{c}} \sum_{j \in \mathcal{N}_i(t)} ((\boldsymbol{q}_i - \hat{\boldsymbol{q}}_j) - (\boldsymbol{p}_i^{\mathrm{d}} - \boldsymbol{p}_j^{\mathrm{d}} - \boldsymbol{d}_{ij})) \end{aligned} \tag{7}$$

Due to $\boldsymbol{d}_{ij} = \boldsymbol{p}_i^{\mathrm{d}} - \boldsymbol{p}_j^{\mathrm{d}}$, then $\boldsymbol{p}_i^{\mathrm{d}} - \boldsymbol{p}_j^{\mathrm{d}} - \boldsymbol{d}_{ij} = 0$. Eq.(7) can be simplified as

$$\begin{aligned} \boldsymbol{u}_i = & -k_{\mathrm{s}} \sum_{j \in \mathcal{N}_i(t)} \phi_{\mathrm{s}}(\| \boldsymbol{p}_{ij} \|) \nabla_{\boldsymbol{p}_i} - k_{\mathrm{a}} \sum_{j \in \mathcal{N}_i(t)} (\boldsymbol{w}_i - \hat{\boldsymbol{w}}_j) - \\ & k_{\mathrm{c}} \sum_{j \in \mathcal{N}_i(t)} (\boldsymbol{q}_i - \hat{\boldsymbol{q}}_j) \end{aligned} \tag{8}$$

Substituting the control law into the dynamics (1) and using the error definitions yields the closed-loop system

$$\begin{cases} \dot{\boldsymbol{q}}_i = \boldsymbol{w}_i \\ \dot{\boldsymbol{w}}_i = -k_{\mathrm{s}} \sum_{j \in \mathcal{N}_i(t)} \phi_{\mathrm{s}}(\| \boldsymbol{q}_{ij} \|) \nabla_{\boldsymbol{q}_i} - k_{\mathrm{a}} \sum_{j \in \mathcal{N}_i(t)} (\boldsymbol{w}_i - \hat{\boldsymbol{w}}_j) - \\ \qquad k_{\mathrm{c}} \sum_{j \in \mathcal{N}_i(t)} (\boldsymbol{q}_i - \hat{\boldsymbol{q}}_j) + \boldsymbol{d}_i(t) \end{cases} \tag{9}$$

where $\boldsymbol{q}_{ij} = \boldsymbol{q}_i - \boldsymbol{q}_j$. This equation clearly shows that the system error dynamics are driven by three components: (1) Potential and consensus forces based on true states; (2) neighbor state estimation errors $\boldsymbol{e}_{p_j}, \boldsymbol{e}_{v_j}$ introduced by event-triggering; (3) external disturbances $\boldsymbol{d}_i(t)$.

3.2 Stability analysis

A candidate Lyapunov function $V(t)$ is constructed to characterize the total energy of the system

$$V(t) = V_1(t) + V_2(t) + V_3(t) \tag{10}$$

where $V_1(t) = \frac{1}{2} \sum_{i=1}^{N} \boldsymbol{w}_i^{\mathrm{T}} \boldsymbol{w}_i$ represents the total kinetic energy; $V_2(t) = \frac{k_{\mathrm{c}}}{2} \sum_{i=1}^{N} \sum_{j \in \mathcal{N}_i} \| \boldsymbol{q}_i - \boldsymbol{q}_j \|^2$ repre-

sents the formation potential energy; $V_3(t)=k_s\sum_{i=1}^{N}\sum_{j\in\mathcal{N}_i}\Psi(\|\boldsymbol{p}_{ij}\|)$, with $\Psi(r)=\int_{r_0}^{r}\phi_s(s)\mathrm{d}s$, represents the collision-avoidance repulsive potential energy.

Computing the derivative of $V_1(t)$, one can obtain

$$\dot{V}_1=\sum_{i=1}^{N}\boldsymbol{w}_i^{\mathrm{T}}\dot{\boldsymbol{w}}_i \tag{11}$$

Substituting the closed-loop control law (9) into Eq.(11), one obtains

$$\dot{V}_1=-\sum_{i=1}^{N}\boldsymbol{w}_i^{\mathrm{T}}\left[k_s\sum_{j\in\mathcal{N}_i(t)}\phi_s(\|\boldsymbol{q}_{ij}\|)\nabla_{\boldsymbol{p}_i}\right]-\sum_{i=1}^{N}\boldsymbol{w}_i^{\mathrm{T}}\left[k_a\sum_{j\in\mathcal{N}_i(t)}(\boldsymbol{w}_i-\hat{\boldsymbol{w}}_j)+k_c\sum_{j\in\mathcal{N}_i(t)}(\boldsymbol{q}_i-\hat{\boldsymbol{q}}_j)\right]-\sum_{i=1}^{N}\boldsymbol{w}_i^{\mathrm{T}}\boldsymbol{d}_i(t) \tag{12}$$

It is worth noting that

$$\boldsymbol{w}_i^{\mathrm{T}}(\boldsymbol{w}_i-\hat{\boldsymbol{w}}_j)=\frac{1}{2}\|(\boldsymbol{w}_i-\boldsymbol{w}_j)\|^2+\frac{1}{2}\|\boldsymbol{w}_i\|^2-\frac{1}{2}\|\boldsymbol{w}_j\|^2-\boldsymbol{w}_i^{\mathrm{T}}\boldsymbol{e}_{\boldsymbol{w}_j} \tag{13}$$

where $\boldsymbol{e}_{\boldsymbol{w}_j}=\boldsymbol{w}_j-\hat{\boldsymbol{w}}_j$ denotes estimated error. Since the graph is undirected, when we sum over all i and j,

$$\sum_i\sum_j\boldsymbol{w}_i^{\mathrm{T}}(\boldsymbol{w}_i-\hat{\boldsymbol{w}}_j)=\frac{1}{2}\sum_{i,j}\|\boldsymbol{w}_i-\boldsymbol{w}_j\|^2-\sum_{i,j}\boldsymbol{w}_i^{\mathrm{T}}\boldsymbol{e}_{\boldsymbol{w}_j}$$

holds true.

For the cross-term

$$\sum_i\sum_j\boldsymbol{w}_i^{\mathrm{T}}(\boldsymbol{q}_i-\hat{\boldsymbol{q}}_j)=\sum_{i,j}(\boldsymbol{w}_i-\boldsymbol{w}_j)^{\mathrm{T}}(\boldsymbol{q}_i-\boldsymbol{q}_j)+\sum_{i,j}\boldsymbol{w}_j^{\mathrm{T}}\boldsymbol{e}_{\boldsymbol{q}_j} \tag{14}$$

where $\boldsymbol{q}_j-\hat{\boldsymbol{q}}_j=(\boldsymbol{q}_j-\boldsymbol{q}_j)+(\boldsymbol{q}_j-\hat{\boldsymbol{q}}_j)=(\boldsymbol{q}_j-\boldsymbol{q}_j)+\boldsymbol{e}_{\boldsymbol{q}_j}$.

Substituting Eqs.(13, 14) into Eq.(12), one obtains

$$\dot{V}_1=-\frac{k_a}{2}\sum_{i=1}^{N}\sum_{j\in\mathcal{N}_i}\|\boldsymbol{w}_i-\boldsymbol{w}_j\|^2+k_c\sum_{i=1}^{N}\sum_{j\in\mathcal{N}_i}\boldsymbol{w}_i^{\mathrm{T}}\boldsymbol{e}_{\boldsymbol{q}_j}-k_a\sum_{i=1}^{N}\sum_{j\in\mathcal{N}_i}\boldsymbol{w}_i^{\mathrm{T}}\boldsymbol{e}_{\boldsymbol{w}_j}-k_c\sum_{i=1}^{N}\sum_{j\in\mathcal{N}_i}(\boldsymbol{w}_i-\boldsymbol{w}_j)^{\mathrm{T}}(\boldsymbol{q}_i-\boldsymbol{q}_j)-\sum_{i=1}^{N}\boldsymbol{w}_i^{\mathrm{T}}\boldsymbol{d}_i-\sum_{i=1}^{N}\boldsymbol{w}_i^{\mathrm{T}}\left[k_s\sum_{j\in\mathcal{N}_i(t)}\phi_s(\|\boldsymbol{q}_{ij}\|)\nabla_{\boldsymbol{p}_i}\right] \tag{15}$$

Similarly, differentiating $V_2(t)$

$$\dot{V}_2=k_c\sum_{i=1}^{N}\sum_{j\in\mathcal{N}_i}(\boldsymbol{q}_i-\boldsymbol{q}_j)^{\mathrm{T}}(\dot{\boldsymbol{q}}_i-\dot{\boldsymbol{q}}_j)=k_c\sum_{i=1}^{N}\sum_{j\in\mathcal{N}_i}(\boldsymbol{q}_i-\boldsymbol{q}_j)^{\mathrm{T}}(\boldsymbol{w}_i-\boldsymbol{w}_j) \tag{16}$$

By taking advantage of the symmetry of undirected graphs

$$\dot{V}_2=2k_c\sum_{i=1}^{N}\boldsymbol{w}_i^{\mathrm{T}}\left(\sum_{j\in\mathcal{N}_i}(\boldsymbol{q}_i-\boldsymbol{q}_j)\right) \tag{17}$$

Similarly, differentiating $V_3(t)$

$$\dot{V}_3=\sum_{i=1}^{N}\sum_{j\in\mathcal{N}_i}\nabla_{\boldsymbol{p}_i}\phi_s(\|\boldsymbol{p}_{ij}\|)^{\mathrm{T}}\dot{\boldsymbol{p}}_i+\nabla_{\boldsymbol{p}_i}\phi_s(\|\boldsymbol{p}_{ij}\|)\dot{\boldsymbol{p}}_j=\sum_{i=1}^{N}\sum_{j\in\mathcal{N}_i}f_{ij}^{\mathrm{rep}}(\boldsymbol{w}_i-\boldsymbol{w}_j) \tag{18}$$

where $f_{ij}^{\mathrm{rep}}=\nabla_{\boldsymbol{p}_i}\phi_s(\|\boldsymbol{p}_{ij}\|)$, by using the symmetry of undirected graphs

$$\dot{V}_3=\sum_{i=1}^{N}\boldsymbol{w}_i^{\mathrm{T}}\sum_{j\in\mathcal{N}_i}f_{ij}^{\mathrm{rep}} \tag{19}$$

Based on the event triggering mechanism and threshold design method, there exists a unified upper bound $\bar{\delta}=\max(\delta_i,\alpha+\delta_{\min})$, such that $\|\boldsymbol{e}_{\boldsymbol{p}_i}\|^2+\gamma\|\boldsymbol{e}_{\boldsymbol{v}_i}\|^2<\delta_i(t)\leqslant\bar{\delta}$ satisfies. Because of $\boldsymbol{e}_{\boldsymbol{p}_i}=\boldsymbol{e}_{\boldsymbol{q}_i}$, $\boldsymbol{e}_{\boldsymbol{v}_i}=\boldsymbol{e}_{\boldsymbol{w}_i}$, and suppose that the estimation error of the neighbor is the same as that of oneself, one has $\|\boldsymbol{e}_{\boldsymbol{q}_i}\|\leqslant\sqrt{\bar{\delta}}$, $\|\boldsymbol{e}_{\boldsymbol{w}_i}\|\leqslant\sqrt{\bar{\delta}/\gamma}$.

By applying Lemma 1, one has

$$\boldsymbol{w}_i^{\mathrm{T}}\boldsymbol{d}_i\leqslant\frac{1}{2\varepsilon_1}\|\boldsymbol{w}_i\|^2+\frac{\varepsilon_1}{2}\|\boldsymbol{d}_i\|^2\leqslant\frac{1}{2\varepsilon_1}\|\boldsymbol{w}_i\|^2+\frac{\varepsilon_1 d_{\max}^2}{2} \tag{20}$$

where the constant $\varepsilon_1>0$.

$$\boldsymbol{w}_i^{\mathrm{T}}\boldsymbol{e}_{\boldsymbol{w}_j}\leqslant\frac{1}{2\varepsilon_2}\|\boldsymbol{w}_i\|^2+\frac{\varepsilon_2}{2}\|\boldsymbol{e}_{\boldsymbol{w}_j}\|^2\leqslant\frac{1}{2\varepsilon_2}\|\boldsymbol{w}_i\|^2+\frac{\varepsilon_2\bar{\delta}}{2\gamma} \tag{21}$$

where the constant $\varepsilon_2>0$.

$$\boldsymbol{w}_i^{\mathrm{T}}\boldsymbol{e}_{\boldsymbol{q}_j}\leqslant\frac{1}{2\varepsilon_3}\|\boldsymbol{w}_i\|^2+\frac{\varepsilon_3}{2}\|\boldsymbol{e}_{\boldsymbol{q}_j}\|^2\leqslant\frac{1}{2\varepsilon_2}\|\boldsymbol{w}_i\|^2+\frac{\varepsilon_3\bar{\delta}}{2} \tag{22}$$

where the constant $\varepsilon_3>0$.

By utilizing Laplace algebraic connectivity, one has

$$\sum_{i=1}^{N}\sum_{j\in N_i}\|\boldsymbol{w}_i-\boldsymbol{w}_j\|^2=2\boldsymbol{w}^{\mathrm{T}}(L\otimes I_3)\boldsymbol{w}\geqslant 2\lambda_2\sum_{i=1}^{N}\|\boldsymbol{w}_i-\bar{\boldsymbol{w}}\|^2 \tag{23}$$

where $\bar{\boldsymbol{w}}=\frac{1}{N}\sum_{i=1}^{N}\boldsymbol{w}_i$ denotes average speed error. Due to $\sum_{i=1}^{N}\|\boldsymbol{w}_i-\bar{\boldsymbol{w}}\|^2=\sum_{i=1}^{N}\|\boldsymbol{w}_i\|^2-N\|\bar{\boldsymbol{w}}\|^2\geqslant 0$, there exists the constant $c_1=2\lambda_2$, satisfying $\sum_{i=1}^{N}\sum_{j\in N_i}\|\boldsymbol{w}_i-\boldsymbol{w}_j\|^2\geqslant c_1\sum_{i=1}^{N}\|\boldsymbol{w}_i\|^2$.

According to Eqs.(15—19), one can obtain

$$\begin{aligned}\dot{V}\leqslant&-\frac{k_a c_1}{2}\sum_{i=1}^{N}\|\boldsymbol{w}_i\|^2+\frac{k_c}{2}\frac{\mathrm{d}}{\mathrm{d}t}\left(\sum_{i=1}^{N}\sum_{j\in N_i}\|\boldsymbol{q}_i-\boldsymbol{q}_j\|^2\right)+\\&\left(\frac{1}{2\varepsilon_1}+\frac{k_a N_{\max}}{2\varepsilon_2}+\frac{k_c N_{\max}}{2\varepsilon_3}\right)\sum_{i=1}^{N}\|\boldsymbol{w}_i\|^2+\\&\left(\frac{\varepsilon_1 N d_{\max}^2}{2}+\frac{k_a N N_{\max}\varepsilon_2\bar{\delta}}{2\gamma}+\frac{k_c N N_{\max}\varepsilon_3\bar{\delta}}{2}\right)\end{aligned} \tag{24}$$

where $N_{\max}=\max|N_i|$ denotes maximum number of neighbors. Therefore, the following inequality holds

$$\dot{V}(t)\leqslant-\theta_1 V_1(t)+\theta_2 V_2(t)+\theta_3 \tag{25}$$

where $\theta_1=\frac{k_a c_1}{2}-\left(\frac{1}{2\varepsilon_1}+\frac{k_a N_{\max}}{2\varepsilon_2}+\frac{k_c N_{\max}}{2\varepsilon_3}\right)$, $\theta_2=2k_c$, $\theta_3=\frac{\varepsilon_1 N d_{\max}^2}{2}+\frac{k_a N N_{\max}\varepsilon_2\delta}{2\gamma}+\frac{k_c N N_{\max}\varepsilon_3\bar{\delta}}{2}$. Due to $V=V_1+V_2+V_3$ and $V_3\geqslant 0$, the inequality holds

$$\dot{V}(t)\leqslant-\theta V(t)+\theta_3 \tag{26}$$

where $\theta=\min(\theta_1,\theta_2)$.

3.3 Exclusion of Zeno behavior

Zeno behavior refers to the occurrence of infinitely many triggering events in finite time, which is physically impossible. We need to prove the existence of a positive constant $\tau_{\min}>0$ such that the inter-event time interval $\tau_k^i\geqslant\tau_{\min}$ for any two consecutive triggers. It is considered that UAVi in $[t_k^i,t_{k+1}^i)$ following any triggering moment t_k^i. At the moment t_k^i, UAVi updates its status estimate to the actual state $\hat{p}_i=p_i(t_k^i)$, $\hat{v}_i=v_i(t_k^i)$. The state estimation error is reset to 0. In $[t_k^i,t_{k+1}^i)$, $\hat{p}_i$ and $\hat{v}_i$ maintain a constant state, meanwhile, $p_i(t)$ and $v_i(t)$ maintain continuous change. The derivative of the state error within this interval is $\dot{e}_{p_i}=-v_i(t)$, $\dot{e}_{v_i}=-u_i(t)-d_i(t)$.

First, the estimated condition of the neighbor $\hat{p}_j$ and $\hat{v}_j$ is the constant in $[t_k^i,t_{k+1}^i)$. The potential function ϕ_s is designed as a smooth function, and when the distance between the drones exceeds the safety distance r_0, the gradient $\nabla\phi_s$ is bounded. If no collision occurs between the drones within a limited time, there exists a positive constant $r_{\min}$ such that $\|p_i(t)-p_j(t)\|\geqslant r_{\min}$, then $\left\|\nabla_{p_i}\phi_s(\|p_{ij}\|)\right\|$ is bounded. Moreover, $p_i(t)$ and $v_i(t)$ will not extend to infinity within a limited time frame. Hence, there exist constants M_p and M_v such that for $t\in[t_k^i,t_{k+1}^i)$, $\|p_i(t)\|\leqslant M_p$ and $\|v_i(t)\|\leqslant M_v$. From the view of Eq.(2), $u_i(t)$ is a continuous function composed of $p_i(t)$ and $v_i(t)$, and each term in the expression is bounded. Hence, there exists the positive constant M_u such that $\|u_i(t)\|\leqslant M_u$. Based on the above boundedness, the inequalities hold

$$\begin{cases}\dfrac{\mathrm{d}}{\mathrm{d}t}\|e_{p_i}(t)\|\leqslant\|\dot{e}_{p_i}(t)\|=\|v_i(t)\|\leqslant M_v\\ \dfrac{\mathrm{d}}{\mathrm{d}t}\|e_{v_i}(t)\|\leqslant\|\dot{e}_{v_i}(t)\|=\|u_i(t)+d_i(t)\|\leqslant M_u+d_{\max}\end{cases} \tag{27}$$

At the initial moment, the error is 0. Integrating Eq.(27), we obtain

$$\begin{cases}\|e_{p_i}(t)\|\leqslant M_v(t-t_k^i)\\ \|e_{v_i}(t)\|\leqslant(M_u+d_{\max})(t-t_k^i)\end{cases} \tag{28}$$

According to Eq.(5), regardless of whether the threshold is in the dynamic mode or the fixed mode, there exists a global positive lower bound $\delta_{\min}^*$. Therefore, the necessary condition for triggering the event is

$$\|e_{p_i}(t)\|^2+\gamma\|e_{v_i}(t)\|^2\geqslant\delta_{\min}^* \tag{29}$$

Substituting Eq.(25) into Eq.(24), one has

$$\begin{cases}\left[M_v(t-t_k^i)\right]^2+\gamma\left[(M_u+d_{\max})(t-t_k^i)\right]^2\geqslant\delta_{\min}^*\\ \left(M_v^2+\gamma(M_u+d_{\max})^2\right)(t-t_k^i)^2\geqslant\delta_{\min}^*\end{cases} \tag{30}$$

$$t-t_k^i<\sqrt{\frac{\delta_{\min}^*}{M_v^2+\gamma(M_u+d_{\max})^2}}\triangleq\tau \tag{31}$$

From Eq.(30), it can be seen that if Eq.(31)

holds true, Eq.(29) cannot be satisfied. Therefore, the time interval between two consecutive triggers must be $\tau > 0$. This rigorously proves the existence of a positive lower bound for the inter-event time, thereby excluding Zeno behavior.

4 Simulation Results

To validate the proposed decentralized control framework with the switching event-triggered communication mechanism, numerical simulations are conducted. It is worth noting that real-world implementations face challenges such as time-varying delays and packet loss. The proposed switching mechanism is designed to be resilient to these issues because the threshold dynamically adjusts to the actual estimation error, rather than relying on fixed timing assumptions.

4.1 Example 1

A swarm of $N=15$ UAVs is considered in a 3D space. The desired formation is a dynamic 3D spiral shape, and the whole formation is moving at a constant speed of $\boldsymbol{v}=[0.8, 0, 0]$ m/s. The initial positions of the UAVs are random around the desired positions of each UAV with radius 1.0 m, and initial velocity perturbation is v at ± 0.2 m/s. The system dynamics follows the double-integrator model (1), integrated with a time step of $\mathrm{d}t=0.01$ s over a total simulation time $T=25$ s.

The control gains are set as $k_s=2.5$, $k_a=3.0$, and $k_s=1.8$ to balance collision avoidance, velocity alignment, and formation cohesion for the complex spiral shape. The safety and communication ranges are $r_0=1.5$ m and $R_{\mathrm{comm}}=8.0$ m, respectively. The main parameters are as follows: The weighting coefficient $\gamma=0.5$; dynamic mode parameters $\alpha=0.1$, $\beta=0.2$, and $\delta_{\min}=0.005$; fixed mode threshold $\delta_f=0.02$; and the switching parameter $\eta=0.3$. As a compromise, this value is selected to preserve a dynamic mode throughout the transient phase, and to transit into a fixed mode upon adequate formation. Bounded external disturbances $\boldsymbol{d}_i(t)$ are modeled as random impulses of magnitude 0.03 occurring with a probability of 0.003 every time step.

Fig.2 shows the complete 3D trajectories of all 15 UAVs as they fly together from loosely scattered initial position into the desired translating spiral formation. A fast convergence phase lasts from 0 to 5 s where all UAVs very quickly converge and organize into an approximate spiral shape and a fine tuning phase lasts from 5 s to 15 s where relative positions are fine-tuned and the formation tracking is formed well.

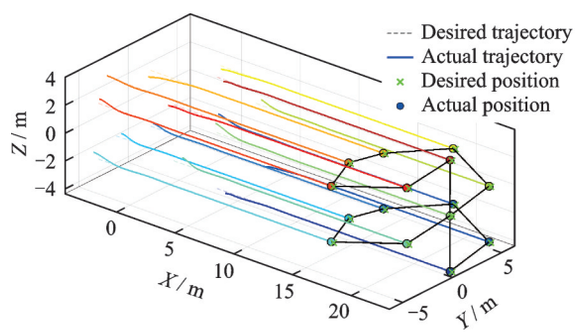

Fig.2 3D formation trajectory

Fig.3 shows that the system starts with the UAVs randomly distributed in the 3D workspace with no obvious structure. The formation error at this initial instant is 0.404, that is, the maximum error from the given configuration of the desired spiral formation. Connecting lines between UAVs, the emergent communication topology based on 8.0 m communication range results in a sparse and irregular network, with the average node degree about 3.2.

Fig.4 presents the error converge feature. The formation error, the velocity error, and the total error converge exponentially, and they converge to steady status after 8 s. The system can rapidly converge, confirming the effectiveness of the algorithm.

Fig.5 illustrates the distribution of inter-event intervals under the switching event-triggered mechanism.The trigger intervals blue markers are symmetrically distributed around 0.18 s, with a mean of 0.181 s and a median of 0.180 s. The consistent interval duration demonstrates the mechanism's stable event timing.

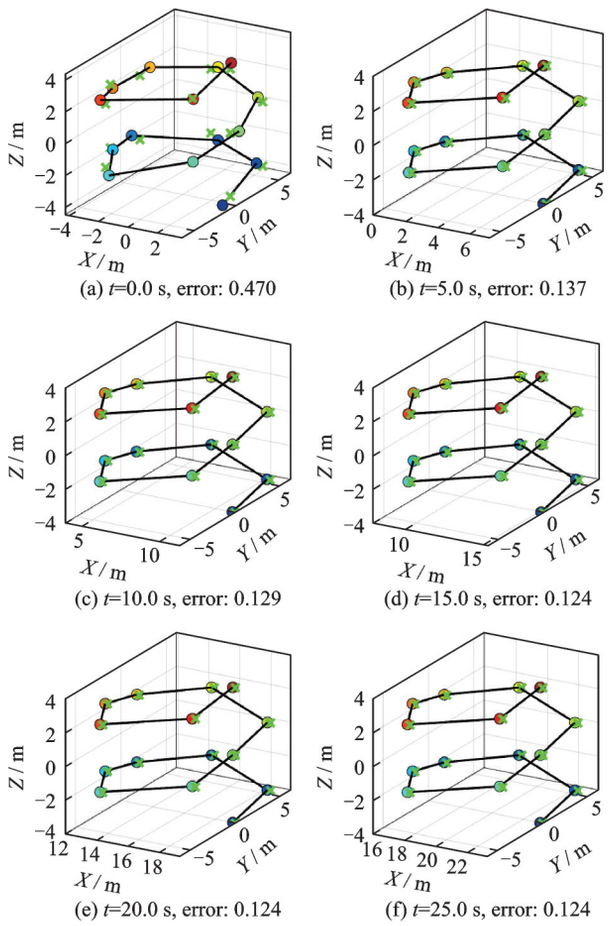

Fig.3 3D formation trajectory segment

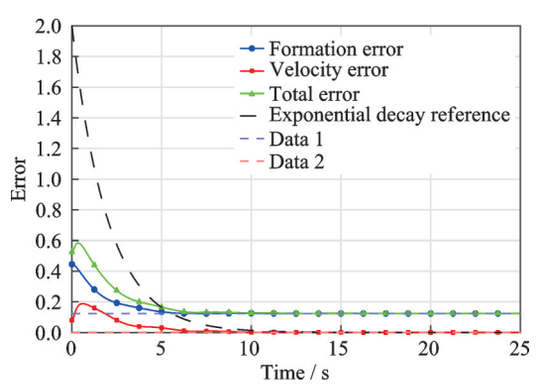

Fig.4 Formation and velocity error trajectory

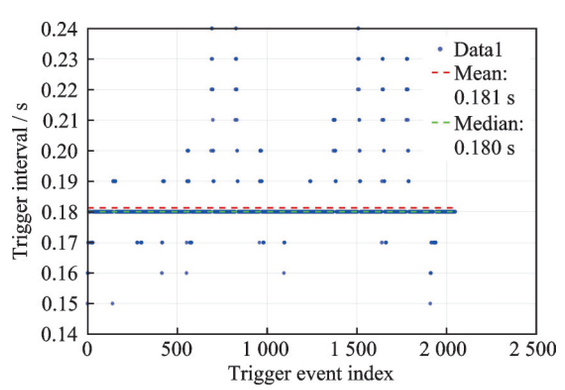

Fig.5 Event-trigger interval analysis

4.2 Example 2

A V-shaped formation in 3D space is deployed by a swarm of $N=10$ UAVs. The dynamic characteristics of the system follow the double integrator model defined in Eq.(1), with a fixed integration time step of $\mathrm{d}t=0.01$ s over the total simulation duration of $T=20$ s. The initial positions of UAVs are randomly perturbed from their nominal formation positions within a sphere of radius of 0.5 m, while initial velocities are initialized as the desired formation velocity $\boldsymbol{v}=[1.0, 0, 0]$ m/s with perturbations on desired formation velocities of ± 0.1 m/s. The parameters of the bio-inspired control law are carefully tuned: Separation gain $k_s=3.0$ is used to avoid collision with a safety radius of $r_0=1.2$ m; alignment gain $k_a=2.5$ is used to push the velocities toward synchronization; and cohesion gain $k_c=2.0$ is used to preserve formation. The communication range is set to $R=6.0$ m, large enough to ensure connectivity for V-formation yet the network topology is sparse. The switching event-triggered mechanism is implemented with the parameters discussed above from theoretical analysis: Weighting coefficient $\gamma=0.5$; dynamic mode parameters $\alpha=0.1$, $\beta=0.3$ and $\delta_{\min}=0.01$; fixed mode threshold $\delta_f=0.02$; and the critical switching parameter $\eta=0.3$. Bounded external disturbances $\boldsymbol{d}_i(t)$ with a magnitude of 0.05 m/s^2 and probability of existence of 0.005 per time step are injected to evaluate robustness under realistic settings.

Fig.6 illustrates the 3D formation trajectories of the multiple UAVs, which explains the motion of each UAV in a collective space. The trajectories exhibit various oscillations at first, but eventually they tend to a stable state and assemble into a formation.

Fig.7 plots the convergence of the formation error and the velocity error over the first 20 s. Both errors have an initial transient, while the formation error converges to about 0.5 and the velocity error is of the order of 0.1. As is seen in 5 s, the rapidly stabilized result shows the effectiveness of the control algorithm in achieving simultaneous formation accuracy and formation consensus in velocity.

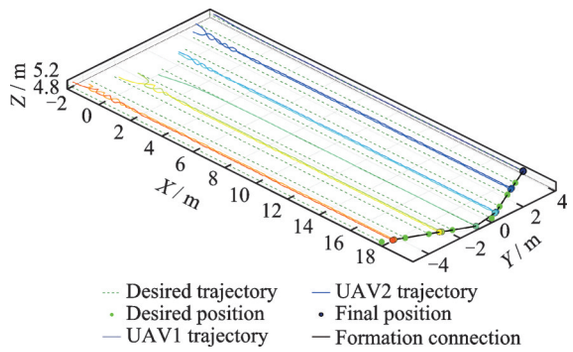

Fig.6 3D UAV swarm formation trajectory

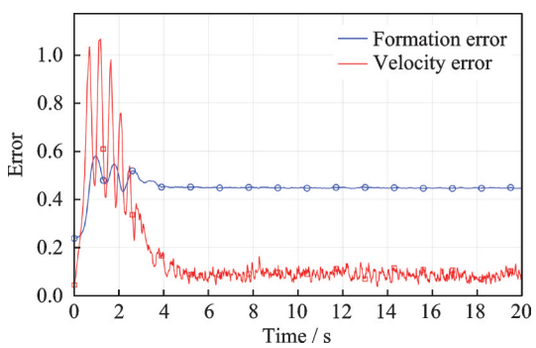

Fig.7 Formation and velocity error convergence

Fig.8 shows the distribution of the number of event triggers on 10 UAVs. UAVs 1 and 6 show very small numbers around 150, while the others maintain normal sizes of around 240. Such a heterogeneous pattern reflects the adaptiveness of the switching event-triggered method, where the communication frequency is time-varying according to local needs.

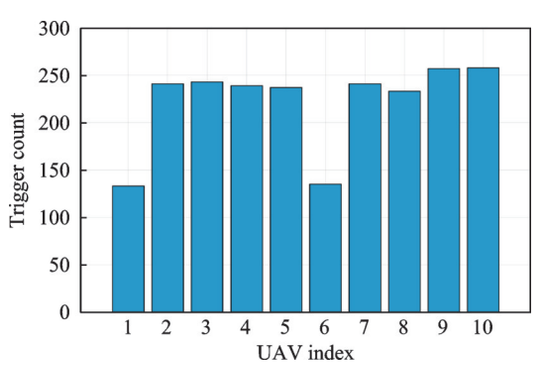

Fig.8 Event trigger statistics per UAV

Fig.9 gives four snapshots of formation evolution at time $t=0.0$, 5.0, 10.0, and 15.0 s. In Figs.9 (a—d), the positions are with actual, desired positions and connecting lines, and the formation error grows from 0.217 m to 0.435 m. From the formation error, it can be seen that the adaptive nature of the system has changed significantly.

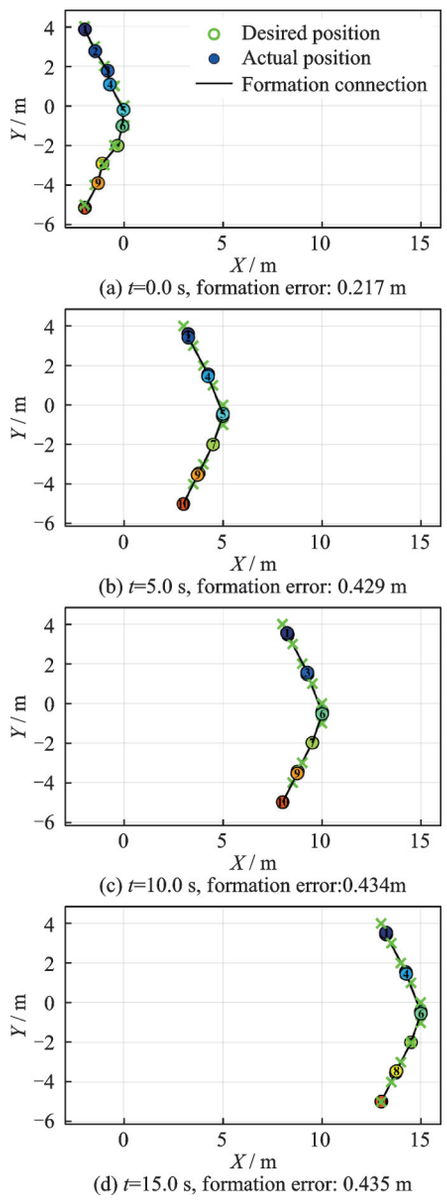

Fig.9 2D formation trajectory segment

Based on the above parameters, six UAVs are selected to simulate and apply the method presented in this paper, and to compare it with the classical event-triggering and elastic event-triggering methods proposed by Dimarogonas et al.[12] and Ren et al.[25]. The selection of core trigger gain can be referred to Table 2. The flexible distributed event trigger parameter settings are as follows. Observer gain is 2; observer trigger threshold coefficient is 0.1; topological recovery time constant is 1. Classic distributed event trigger parameters are set as: Threshold

parameter is 0.6, and design parameter is 0.15. The frequency of the cycle time triggering mechanism is 20 Hz. Communication frequency and efficiency are shown in Table 3. The event-triggered framework of the proposed switching mode triggered only 93 times throughout the entire simulation process, which is 94.2% less than 1 602 times triggered by the periodic triggering. This number is also significantly lower than 728 times of the classical event triggering and 479 times of the elastic distributed event triggering. Therefore, the proposed method achieves the highest average trigger interval, indicating that the UAV maintains consistency while significantly reducing the communication frequency.

Table 2 Parameter configuration

Method	Parameter 1	Parameter 2	Physical interpretation	Tuning range searched
Time trigger	k_a=0.2	—	Gain	$k_a \in [0.1,5]$
Ref.[12]	γ_1=0.6	γ_2=0.3	Threshold gain	$\gamma \in [0.1,5]$
Ref.[25]	r=0.4	ε=5	Decay factor	$r \in [0.2,1]$
Proposed method	α=0.5	δ_f=0.1	Convergence speed/Comm. Rate	$\alpha \in [0.1,2]$

Table 3 Comparison of four performance algorithms

Method	Trigger count	Average interval	Formation RSME	Velocity RSME
Time trigger	1 602	0.056 1	2.430 2	0.588 4
Ref.[12]	728	0.117 1	7.468 0	3.461 9
Ref.[25]	479	0.167 3	7.799 7	1.517 0
Proposed method	93	0.927 2	6.479 4	0.135 9

In terms of formation accuracy, the periodic triggering mechanism performs the best with an error of 2.430. The proposed method shows a higher error of 6.749. This also indicates that there is some loss in absolute position accuracy during the pursuit of reducing communication volume. However, in terms of indicators, the proposed method is still superior to the classical event triggering and elastic distributed event triggering. Fortunately, one of the key advantages of the proposed method is that it achieves the lowest speed consistency of RMSE of 0.136, which is less than 1/4 of that of the periodic triggering error, and several orders of magnitude higher than that of the classical event triggering mechanism. This result also highlights the effectiveness of the bionic alignment mechanism within the switching framework, maintaining coordinated group movement even in the case of sparse communication.

5 Conclusions

In this paper, a decentralized control method for UAV swarm using the self-organizing concepts of starling flocks has been presented. This approach combines separation, alignment and cohesion behaviors into a completely distributed, leaderless control law based entirely on local behaviors. Besides, an adaptive switching event-triggered communication protocol has been proposed, which dramatically reduces communication time and reliably ensures formation stability and swarm interaction. Lyapunov-based analysis guarantees uniform ultimate boundedness of the closed-loop system. The simulation results also confirm the efficacy of the proposed method to achieve velocity consensus with low communication.

References

[1] AHMAD T, MOREL A, CHENG N, et al. Future UAV/drone systems for intelligent active surveillance and monitoring[J]. ACM Computing Surveys, 2026, 58(2): 1-37.

[2] LIU Y H, LIU Z H, WANG G Z, et al. Flexible multi-UAV formation control via integrating deep reinforcement learning and affine transformations[J]. Aerospace Science and Technology, 2025, 157: 109812.

[3] LI K X, FAN H D, YANG Y D, et al. Multiagent reinforcement-learning-based AAV path and resource allocation for ground-to-air communication network[J]. IEEE Internet of Things Journal, 2025, 12(21): 44243-44254.

[4] BALLERINI M, CABIBBO N, CANDELIER R, et al. Empirical investigation of starling flocks: A benchmark study in collective animal behaviour[J]. Animal Behaviour, 2008, 76(1): 201-215.

[5] REYNOLDS C W, REYNOLDS C W. Flocks, herds and schools: A distributed behavioral model[C]//Proceedings of the 14th Annual Conference on Computer Graphics and Interactive Techniques. [S. l.]: ACM, 1987: 25-34.

[6] OLFATI-SABER R. Flocking for multi-agent dynamic systems: Algorithms and theory[J]. IEEE Transactions on Automatic Control, 2006, 51(3): 401-420.

[7] LU J, ZHAO J Y, NIU J D. Boids-based integration algorithm for formation control and obstacle avoidance in unmanned aerial vehicles[J]. Machines, 2025, 13(4): 255.

[8] MONTANARI A N, BARIONI A E D, DUAN C, et al. Optimal flock formation induced by agent heterogeneity[J]. Nature Communications, 2025, 16: 9626.

[9] MA K, ZHAO H Y, WANG J, et al. A multi-UAV network formation scheme via integrated localization and motion planning[J]. IEEE Transactions on Network Science and Engineering, 2025, 12(3): 1552-1566.

[10] KHODAVERDIAN M, NAJAFI M, KAZEMIFAR O, et al. Fault-tolerant model predictive sliding mode control for trajectory replanning of multi-UAV formation flight[J]. Applied Mathematics and Computation, 2025, 487: 129073.

[11] ZHOU Z X, FENG X X, PAN F, et al. Receding horizon control for UAV formation reconfiguration: An enhanced marine predators strategy[J]. IEEE Transactions on Automation Science and Engineering, 2025, 22: 15904-15915.

[12] DIMAROGONAS D V, FRAZZOLI E, JOHANSSON K H. Distributed event-triggered control for multi-agent systems[J]. IEEE Transactions on Automatic Control, 2012, 57(5): 1291-1297.

[13] WANG X L, KONG L H, MENG T T, et al. Event-triggered tracking control for a flapping-wing aerial vehicle with prescribed performance[J]. IEEE Transactions on Aerospace and Electronic Systems, 2025, 61(6): 17476-17487.

[14] MEI Y, LI F, XIA R S, et al. Fixed-time adaptive neural tracking control for nonstrict-feedback nonlinear systems with mismatched disturbances using an event-triggered scheme[J]. Nonlinear Dynamics, 2023, 111(6): 5383-5400.

[15] KONG L H, REIS J, HE W, et al. Event-triggered prescribed-time tracking control for UAVs using polynomial error trajectories[J]. IEEE Transactions on Automation Science and Engineering, 2025, 22: 16476-16486.

[16] MA J, CHEN X Y, WEN G H, et al. Dynamic memory event-triggered lag consensus of multi-UAV systems with hybrid attacks over stochastic switching topology[J]. IEEE Transactions on Automation Science and Engineering, 2025, 22: 16999-17009.

[17] SHI Y Y, LI J, LV M L, et al. Event-based fuzzy asynchronous consensus for UAV swarm under jointly connected digraphs[J]. IEEE Transactions on Fuzzy Systems, 2025, 33(9): 3195-3209.

[18] LI B H, GAO Q, WANG Z Q, et al. Adaptive consensus in multi-agent systems employing event-driven communication under actuator and sensor attacks[J]. Guidance, Navigation and Control, 2025, 5(2): 221-233.

[19] LIAO Z R, SHI J, WANG S P, et al. Self-triggering secure consensus against adversarial attacks[J]. Guidance, Navigation and Control, 2025, 5(2): 173-184.

[20] DING H H, LIANG T H, PING Y Q, et al. Adaptive communication and control co-design for remote UAV systems[C]//Proceedings of 2025 IEEE 101st Vehicular Technology Conference (VTC2025-Spring). Oslo, Norway: IEEE, 2025: 1-6.

[21] ABBASI M, MARQUEZ H J. Dynamic event-triggered formation control of multi-agent systems with non-uniform time-varying communication delays[J]. IEEE Transactions on Automation Science and Engineering, 2025, 22: 8988-9000.

[22] XU B, LI Y X, HOU Z S, et al. Dynamic event-triggered reinforcement learning-based consensus tracking of nonlinear multi-agent systems[J]. IEEE Transactions on Circuits and Systems Ⅰ: Regular Papers, 2023, 70(5): 2120-2132.

[23] ZHAO G L, HUA C C, GUAN X P. A hybrid event-triggered approach to consensus of multiagent systems with disturbances[J]. IEEE Transactions on Control of Network Systems, 2020, 7(3): 1259-1271.

[24] YIN T T, GU Z, XIE X P. Observer-based event-triggered sliding mode control for secure formation tracking of multi-UAV systems[J]. IEEE Transactions on Network Science and Engineering, 2023, 10(2): 887-898.

[25] REN Y X, WANG J, ZHANG J. Resilient distributed event-triggered formation control for multi-UAV systems under DoS attacks[J]. IEEE Systems Journal, 2025, 19(4): 1259-1269.

[26] SHI S, WU S Q, WEI B. Neural-network-based event-triggered formation tracking for nonlinear multi-UAV systems with switching topologies under DoS attacks[J]. IEEE Transactions on Automation Science and Engineering, 2025, 22: 11656-11667.

[27] HUANG Y, XU X F, MENG Z Y, et al. A smooth distributed formation control method for quadrotor UAVs under event-triggering mechanism and switching topologies[J]. IEEE Transactions on Vehicular Technology, 2025, 74(7): 10081-10091.

[28] LIU P M, GUO X G, WANG J L, et al. Conditional disturbance compensation-based fault-tolerant group consensus control for MASs: An event-based switching method[J]. IEEE Transactions on Automation Science and Engineering, 2025, 22: 13828-13841.

[29] QIAN H J, WEI L. Non-lipschitz continuous stabilizers for nonlinear systems with uncontrollable unstable linearization[J]. Systems & Control Letters 2001, 42(3): 185-200.

Acknowledgements This work was supported in part by the National Natural Science Foundation of China (Nos. 624B2013, 62350048, U2541218, T2121003, 62533006). The authors would like to acknowledge the following people for their assistance: HUO Mengzhen, WEI Chen, SUN Yongbin, WANG Siyuan, and YUAN Yang, all with the National Key Laboratory of Aircraft Integrated Flight Control, School of Automation Science and Electrical Engineering, Beihang University.

Authors

The first author Mr. **MEI Yu** received his M.S. degree in electrical engineering and automation from the Anhui University of Technology, Ma'anshan, China, in 2023. He is currently pursuing the Ph.D. degree in Beihang University of Aeronautics and Astronautics, Beijing, China. His current research interests include Bionic unmanned aerial vehicle swarm control, nonlinear control, chaotic system.

The corresponding author Prof. **DUAN Haibin** received his Ph.D. degree in control theory and engineering from Nanjing University of Aeronautics and Astronautics in 2005. He is a full professor with School of Automation Science and Electrical Engineering, Beihang University, Beijing, China. He is the Head of the Bio-inspired Autonomous Flight Systems (BAFS) Research Group, Beihang University, Beijing, China. His current research interests are multi-UAV swarm autonomous control, bio-inspired intelligence, and biological computer vision.

Author contributions Mr. **MEI Yu** designed the study, compiled the models, conducted the analysis and wrote the manuscript. Prof. **DUAN Haibin** contributed to the discussion and background of the study. Both authors commented on the manuscript draft and approved the submission.

Competing interests The authors declare no competing interests.

(Production Editor: ZHANG Bei)

基于欧椋鸟群聚集机制的无人机分散式协同控制

梅 宇，段海滨

(北京航空航天大学自动化科学与电气工程学院飞行器一体化控制全国重点实验室，北京 100083，中国)

摘要：针对当前无人机集群协同控制中通信负载与动态稳定性难以兼顾的瓶颈，本文旨在借鉴自然界椋鸟群的涌现性集体行为，设计一种分布式且无领导者的新型控制策略。通过模拟椋鸟群“分离—对齐—聚合”的自组织机理，构建仅依赖局部交互的控制律，并创新性地引入自适应切换的事件触发通信机制，以突破传统周期通信的带宽限制。结合李雅普诺夫稳定性理论，严格推导并证明了该策略在外界扰动下的鲁棒性边界，确保系统误差收敛于有界范围。数值仿真结果表明，该方法不仅能显著降低通信负担，还能在动态过渡阶段维持优异的瞬态性能与集群几何构型的稳定。本研究证实了生物启发式协同机制与自适应事件触发策略融合的有效性，揭示了资源受限条件下分布式集群系统的稳定性原理，为大规模无人机集群在物流配送及协同侦察等资源敏感型场景的落地应用提供了重要的理论依据。

关键词：欧椋鸟群；分散控制；切换事件触发通信；无人集群控制

研究亮点：

1. 针对无人机集群在编队稳定性与通信效率之间面临的严峻权衡问题，本文提出了一种融合椋鸟群自组织机理与切换式事件触发控制机制的统一去中心化控制范式。

2. 本文提出了一种新型切换事件触发机制并完成了理论证明。与依赖周期通信或固定阈值的传统方案不同，本协议通过感知实时聚合需求，实现了通信资源的自适应动态调配。